

ChemComm

Accepted Manuscript



This is an *Accepted Manuscript*, which has been through the Royal Society of Chemistry peer review process and has been accepted for publication.

Accepted Manuscripts are published online shortly after acceptance, before technical editing, formatting and proof reading. Using this free service, authors can make their results available to the community, in citable form, before we publish the edited article. We will replace this *Accepted Manuscript* with the edited and formatted *Advance Article* as soon as it is available.

You can find more information about *Accepted Manuscripts* in the [Information for Authors](#).

Please note that technical editing may introduce minor changes to the text and/or graphics, which may alter content. The journal's standard [Terms & Conditions](#) and the [Ethical guidelines](#) still apply. In no event shall the Royal Society of Chemistry be held responsible for any errors or omissions in this *Accepted Manuscript* or any consequences arising from the use of any information it contains.

COMMUNICATION

Bright CuInS₂/CdS Nanocrystal Phosphors for High-Gain Full-Spectrum Luminescent Solar Concentrators

Cite this: DOI: 10.1039/x0xx00000x

Received 00th February 2015,
Accepted 00th February 2015

DOI: 10.1039/x0xx00000x

www.rsc.org/

Kathryn E. Knowles,^a Troy B. Kilburn,^a Dane G. Alzate,^a Stephen McDowall,^b and Daniel R. Gamelin^{a*}

The performance of colloidal CuInS₂/CdS nanocrystals as phosphors for full-spectrum luminescent solar concentrators has been examined. Their combination of large solar absorption, high photoluminescence quantum yields, and only moderate reabsorption produces the highest projected flux gains of any nanocrystal luminophore to date.

Luminescent solar concentrators (LSCs) collect and concentrate solar energy through absorption of incident photons by luminophores, followed by emission into a waveguide that directs the emitted photons onto photovoltaic (PV) cells.^{1,2} LSCs can be made in a variety of configurations,²⁻⁵ the most common of which comprises a two-dimensional planar waveguide with edge-mounted PVs.^{2,6} LSCs have the potential to reduce the cost of solar energy by allowing replacement of expensive large-area PVs with cheaper solar-harvesting antennae coupled to small PVs.^{1,2} LSCs may also allow integration of solar technologies into other existing architectures, such as windows, without compromising their primary function.² Different applications will demand different tailored luminophores, but the achievement of commercial viability in any LSC configuration still requires new luminophores that are bright, stable, and do not reabsorb their own luminescence.^{2,7}

Semiconductor nanocrystals (NCs) are a promising class of LSC luminophore due to their tuneable absorption spectra, solution processability, photostability, and high photoluminescence (PL) quantum yields.⁸⁻¹⁶ Unlike molecular luminophores, which often have relatively narrow absorption bands,^{6,17,18} semiconductor NCs absorb broadly at all energies greater than their (tuneable) band gap. Such broad absorption is advantageous for applications seeking to capture as much of the solar spectrum as possible. Most NCs suffer from significant overlap between their absorption and PL spectra, however.^{8,9,11} Recently, we demonstrated that NCs containing luminescent impurities exhibit very small reabsorption losses at application-relevant optical densities (*e.g.*, OD = 1 across the device thickness) and photon-transport lengths (*e.g.*, up to 1.2 m) because

dopant-centered emission in these NCs occurs at much lower energies than the band gap of the host NC.¹⁶ Quantitative measurements¹⁶ showed that doped NCs have smaller intrinsic reabsorption losses than heterostructured NCs with large apparent Stokes shifts.^{13,14,19} Of the NCs investigated, Cd_{0.999}Cu_{0.001}Se NCs were identified as the “best in class” luminophores for full-spectrum LSCs because of their large solar absorption and small reabsorption losses, but their relatively low PL quantum yields ($\eta_{PL} \leq 0.4$) still limit their overall performance. Here, we use the experimental and theoretical tools developed in our previous study to quantify the LSC performance of high-quantum-yield CuInS₂/CdS core/shell NCs ($\eta_{PL} = 0.86$), and compare these NCs to the leading heterostructured and doped NC phosphors examined previously for full-spectrum applications. The high PL quantum yield and large solar absorption of CuInS₂/CdS NCs lead to exceptionally high projected flux gains for planar LSCs coupled to Si PVs, exceeding those of Cd_{0.999}Cu_{0.001}Se NCs by over a factor of two at all LSC length scales. Routes for further improvement are discussed.

To maximize the flux gain of an LSC based on CuInS₂/CdS NCs, we aimed to synthesize bright CuInS₂/CdS NCs with absorption and PL spectra that have maximal overlap with the solar spectrum and the external quantum efficiency (EQE) spectrum of a crystalline Si (c-Si) solar cell, respectively. CuInS₂/CdS NCs were synthesized following literature procedures²⁰ with minor modifications (see SI for details). Figure 1A shows the absorption spectrum of a concentrated solution of CuInS₂/CdS NCs measured over a 1-mm pathlength and a PL spectrum of the same solution diluted by a factor of 100. These CuInS₂/CdS NCs have their first absorption peak centered at $\lambda_{\text{thresh}} = 570$ nm, a broad PL spectrum centered at 765 nm, and $\eta_{PL} = 0.86 \pm 0.02$. Their Cu:In:Cd ratio is 1.00:1.06:1.23 as measured by inductively coupled plasma atomic emission spectroscopy, and their average diameter is 3.1 ± 0.5 nm as measured by TEM (see SI for details). Based on these measurements, the thickness of the CdS shell is ~ 0.3 nm and the diameter of the CuInS₂ core is ~ 2.5 nm, which is consistent with the average crystalline domain sizes of 2.6 and 3.4 nm estimated from the line-widths of powder X-ray diffraction spectra of the CuInS₂ cores and

CuInS₂/CdS core/shell NCs, respectively (see SI). As reported previously,²⁰ CuInS₂/CdS NCs made by this method are reproducibly bright for a range of band gap energies down to that represented in Figure 1A. For example, absorption and PL spectra of another CuInS₂/CdS NC sample that has $\eta_{PL} = 0.87 \pm 0.02$ but a larger band gap ($\lambda_{\text{thresh}} = 530$ nm) are shown in the Supplementary Information. We focus on the CuInS₂/CdS NCs of Figure 1A, which have the same high η_{PL} , absorb 11% more solar photons (as calculated by the overlap integral of the absorption spectrum and the AM1.5 solar spectrum), and also still have their entire PL spectrum between 480 and 1000 nm, where the EQE of a c-Si solar cell exceeds 95% (Figure 1B).²¹ CuInS₂/CdS NCs with band gaps narrower than in Figure 1A (*i.e.*, larger diameters) absorb even more solar photons but re-emit a significant fraction of these photons beyond 1000 nm, where c-Si is less sensitive (see below). Narrowing the PL band could, in principle, ameliorate this issue, but the PL line width in Figure 1A derives primarily from strong electron-phonon coupling in the luminescent excited state and is likely close to its homogeneous value.

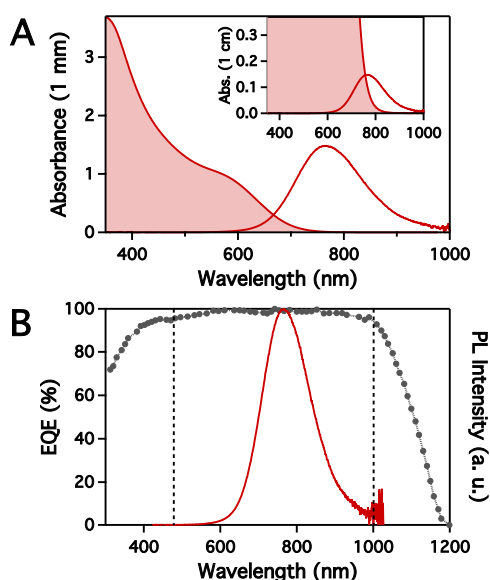


Fig. 1. **A** Absorption (solid line with shading) and PL spectra of CuInS₂/CdS core/shell nanocrystals dispersed in tetrachloroethylene. The absorption spectrum was collected over a 1 mm pathlength. Inset: Projected absorption spectrum of the same nanocrystal solution over a 1-cm pathlength. The PL spectra in both plots were taken of a 100-fold dilution of the solution used to obtain the absorption spectra. **B** PL spectrum of the CuInS₂/CdS NCs from **A** (red solid line) plotted with the external quantum efficiency (EQE) spectrum of a c-Si solar cell from ref. 21 (gray circles). The vertical dashed lines indicate the region of the EQE spectrum where EQE \geq 95%.

The relatively large difference in energy between the absorption and PL peaks in Figure 1A is due to deep trapping in the luminescent excited state,^{20,22-24} a process closely related to that in dilute activator-doped semiconductor phosphors. Despite this large separation, the broad widths of these absorption and PL bands still lead to significant overlap and hence reabsorption losses. The absorption/PL overlap becomes more obvious over longer optical pathlengths, for example the 1 cm pathlength of Figure 1A, inset. Our aim here is to assess the impact of such overlap on the performance of these NCs as LSC luminophores.

The probability that an emitted photon will be reabsorbed over a given photon transport distance in an LSC can be predicted from a luminophore's absorption and PL spectra using equation 1.¹⁶

$$R(l) = \int PL_{norm}(\lambda)(1 - 10^{-A_{norm}(\lambda)l})d\lambda \quad (1a)$$

$$l = \frac{L \cdot OD_t}{t} \quad (1b)$$

Here, $PL_{norm}(\lambda)$ is the PL spectrum normalized by area, $A_{norm}(\lambda)$ is the absorption spectrum normalized at λ_{thresh} , and l is the reduced pathlength defined in equation 1b by the photon transport distance, L , the transverse optical density of the LSC at λ_{thresh} , OD_t , and the device thickness, t .¹⁶ Use of a reduced pathlength allows comparison of predicted reabsorption probabilities with experimental luminescence attenuation values measured under different conditions (*e.g.*, different luminophore concentrations or LSC configurations).

Figure 2A plots the predicted reabsorption probability, $R(l)$, versus reduced LSC pathlength, l , calculated for CuInS₂/CdS NCs using the spectra from Figure 1A (note the inverted y axis). For comparison, Figure 2A also plots $R(l)$ values predicted for the leading doped (Cd_{0.999}Cu_{0.001}Se) and heterostructured (CdSe/CdS core/shell) NC luminophores.¹⁶ At small l , the effect of reabsorption is more pronounced in the CuInS₂/CdS NCs than in the other two NCs shown in Figure 2A, which both display more monotonic increases in $R(l)$ with increasing l . Notably, however, the slope of $R(l)$ is smallest for the CuInS₂/CdS NCs at large l , causing $R(l)$ for these NCs to eventually cross both the CdSe/CdS core/shell and Cd_{0.999}Cu_{0.001}Se $R(l)$ curves (at $l = 164$ and 1234, respectively, see SI). A useful metric for quantifying reabsorption is the parameter $R_{1/2}$, defined as the reduced pathlength at which $R(l) = 0.5$.¹⁶ $R_{1/2}$ provides a concise summary of the curves shown in Figure 2A and is useful for comparing reabsorption across NCs, albeit with obvious sacrifices in insight. $R_{1/2} = 43$ for the CuInS₂/CdS NCs, compared to $R_{1/2} = 320$ and 92 for the Cd_{0.999}Cu_{0.001}Se and CdSe/CdS NCs, respectively.¹⁶

To test the predictions of equation 1, the solution of CuInS₂/CdS NCs used to obtain the absorption spectrum in Figure 1A was loaded into a 120-cm liquid waveguide that is fiber-coupled to a spectrometer at one end, and PL was measured as a function of the distance (L) between the collection end of the waveguide and a translatable 385-nm LED excitation source. This one-dimensional liquid waveguide device, or "1D LSC", has a total thickness of 1.65 mm (1 mm liquid and 0.65 mm quartz) and, once loaded with the CuInS₂/CdS NC solution, an $OD_t = 1$ at $\lambda_{\text{thresh}} = 570$ nm. Figure 2B shows PL spectra of these CuInS₂/CdS NCs measured at various excitation distances in the 1D LSC. The apparent red shift in the PL spectra with increasing L demonstrates how reabsorption primarily attenuates the higher-energy luminescence. To approximate the PL spectrum at $L = 0$ in the 1D LSC, we measured the PL spectrum of a 100-fold diluted solution of CuInS₂/CdS NCs (*i.e.*, $OD_t = 0.01$) at $L = 1$ cm and scaled it such that its intensity matched the intensity of the PL spectrum for the $OD_t = 1$ solution at $L = 1$ cm from 850-1050 nm, where reabsorption losses are negligible. This projected $L = 0$ spectrum is the purple spectrum in Figure 2B. Figure 2C plots the spectrally integrated PL intensity versus L for the CuInS₂/CdS NCs measured here and previously reported data for Cd_{0.999}Cu_{0.001}Se and CdSe/CdS NCs.¹⁶ The data in Figure 2C are normalized at $L = 0$ and corrected for waveguide losses to focus

specifically on the properties of the phosphors. The uncorrected data are qualitatively similar to the corrected data, and are shown in the SI. The remarkable qualitative similarity between the experimental data in Figure 2C and the predicted curves in Figure 2A demonstrates the predictive power of equation 1. To compare the curves in Figure 2C quantitatively, we define the parameter $L_{1/2}$ to be the excitation distance L at which the integrated PL intensity is 50% of its value at $L = 0$. Similar to the trend in $R_{1/2}$, the $\text{CuInS}_2/\text{CdS}$ NCs have a smaller $L_{1/2}$ value ($L_{1/2} = 9$ cm) than both $\text{Cd}_{0.999}\text{Cu}_{0.001}\text{Se}$ ($L_{1/2} = 42$ cm) and CdSe/CdS NCs ($L_{1/2} = 12$ cm),¹⁶ but the integrated PL intensity of $\text{CuInS}_2/\text{CdS}$ NCs is still significant at $L = 120$ cm.

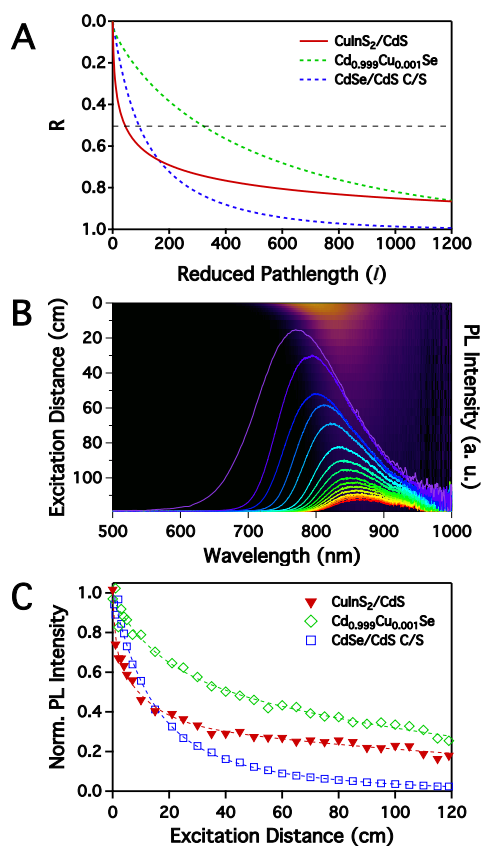


Fig. 2. A Reabsorption probability, R , calculated from eq. 1 and plotted versus reduced pathlength, l , for $\text{CuInS}_2/\text{CdS}$ (solid red line), $\text{Cd}_{0.999}\text{Cu}_{0.001}\text{Se}$ (dashed green line), and CdSe/CdS (dashed blue line) NCs. B Two-dimensional plot of PL intensity versus wavelength and excitation distance overlaid with PL spectra of the $\text{CuInS}_2/\text{CdS}$ NCs collected at various excitation distances in the 1D LSC. C Plot of spectrally integrated PL intensity corrected for waveguide losses and normalized at $L = 0$ versus excitation distance (L) for $\text{CuInS}_2/\text{CdS}$ (filled red triangles), $\text{Cd}_{0.999}\text{Cu}_{0.001}\text{Se}$ (open green diamonds), and CdSe/CdS (open blue squares) NCs. The dotted lines are guides for the eye. Data for $\text{Cd}_{0.999}\text{Cu}_{0.001}\text{Se}$ and CdSe/CdS core/shell nanocrystals shown in A and C are taken from ref. 16 and included for comparison.

In addition to reabsorption, the overall performance of an LSC luminophore is also governed by its ability to absorb solar photons and its PL quantum yield. All three properties contribute to the flux gain (FG) of an LSC device. The flux gain is the factor by which the LSC increases the output of a particular PV cell or set of cells.¹⁵ Equation 2 defines the flux gain of our experimental 1D LSC device coupled to c-Si PV cells at each end, as a function of length, L .¹⁶

$$FG = G_{geo}(L)\eta_{EC}\frac{\eta_{PV}^{PL}}{\eta_{PV}^{AM1.5}}\eta_{PL}\frac{A_{Sol,NC}}{A_{Sol,PV}}\int_0^L I_{PL}(L)dL \quad (2)$$

In equation 2, $G_{geo}(L)$ is the geometric gain, η_{EC} is the fraction of emitted photons not lost to the waveguide's escape cones defined by Snell's law, η_{PV}^{PL} and $\eta_{PV}^{AM1.5}$ are the efficiencies of a c-Si PV illuminated by the PL of the NCs and AM1.5 solar radiation, respectively, $A_{Sol,NC}$ and $A_{Sol,PV}$ are the incident solar photon flux absorbed by the NCs and PV, respectively, and $I_{PL}(L)$ is the experimental integrated PL intensity measured at excitation distance L in the 1D LSC. For our 1D LSC device, $\eta_{EC} \sim 0.5$ due to the presence of both horizontal and vertical escape cones,¹⁶ and the ratio $\eta_{PV}^{PL}/\eta_{PV}^{AM1.5} \sim 1$ since the reference c-Si PV cell has a reported external quantum efficiency $\geq 95\%$ from 480 to 1000 nm (Figure 1B).²¹ For the $\text{CuInS}_2/\text{CdS}$ NCs reported here, $\eta_{PL} = 0.86$ and $A_{Sol,NC} = 9.2 \times 10^{20}$ photons/m²s. $A_{Sol,PV} = 24.8 \times 10^{20}$ photons/m²s for a c-Si solar cell. Equation 2 was previously verified by a direct measurement of the flux gain of our 1D LSC under natural sunlight.¹⁶

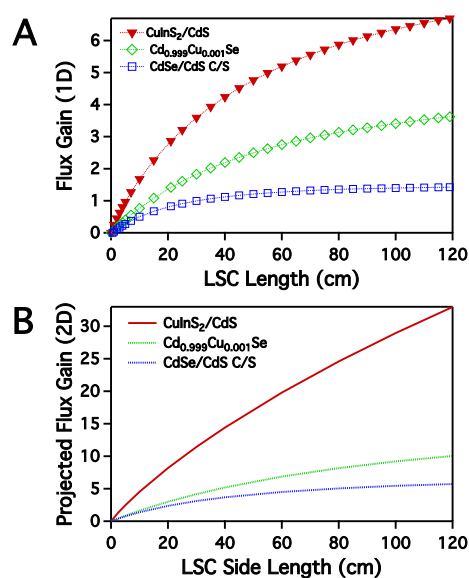


Fig. 3. Flux gains for $\text{CuInS}_2/\text{CdS}$ NC LSCs coupled to c-Si photovoltaics and illuminated with AM 1.5 solar irradiation. Flux gains are plotted versus LSC length and side length, respectively, for **A** the one-dimensional measurement device (calculated using eq. 2 and experimental data from Figure 2B) and **B** hypothetical square planar LSC devices. Results for $\text{Cd}_{0.999}\text{Cu}_{0.001}\text{Se}$ and CdSe/CdS core/shell NCs taken from ref. 16 are included for comparison. The dotted lines in A are guides for the eye.

Figure 3A plots the flux gain calculated from equation 2 versus LSC length for the 1D LSC containing $\text{CuInS}_2/\text{CdS}$, $\text{Cd}_{0.999}\text{Cu}_{0.001}\text{Se}$, or CdSe/CdS NCs. Of the three NCs shown here, the $\text{CuInS}_2/\text{CdS}$ NCs have both the largest η_{PL} (0.86 compared to 0.27 and 0.68 for $\text{Cd}_{0.999}\text{Cu}_{0.001}\text{Se}$ and CdSe/CdS , respectively) and absorb the most solar photons (9.2×10^{20} photons/m²s compared to 8.9×10^{20} and 3.3×10^{20} photons/m²s for $\text{Cd}_{0.999}\text{Cu}_{0.001}\text{Se}$ and CdSe/CdS , respectively). These two properties compensate for larger reabsorption losses, and lead the $\text{CuInS}_2/\text{CdS}$ NCs to produce the greatest 1D flux gains at all length scales.

With these results in hand, it is now possible to project the flux gains for square "2D" LSC devices made from these $\text{CuInS}_2/\text{CdS}$ NCs with $t = 1$ mm, $OD_t = 1$, and c-Si PVs attached to all four edges. 2D flux gains were calculated using methods described previously,¹⁶ with

the same luminophore and PV parameters used in eq. 2. Figure 3B plots the projected 2D flux gain versus LSC side length for $\text{CuInS}_2/\text{CdS}$, $\text{Cd}_{0.999}\text{Cu}_{0.001}\text{Se}$, and CdSe/CdS NCs. These curves exhibit the same qualitative trends as the 1D flux gain curves shown in Figure 3A. Importantly, the projected flux gain for a 120 cm x 120 cm device containing these $\text{CuInS}_2/\text{CdS}$ NCs is 33, which is 3.3 times larger than the projected flux gain for the same device containing $\text{Cd}_{0.999}\text{Cu}_{0.001}\text{Se}$ NCs.¹⁶ Since η_{PL} is a factor 3.2 larger for $\text{CuInS}_2/\text{CdS}$ NCs than for $\text{Cd}_{0.999}\text{Cu}_{0.001}\text{Se}$ NCs, and $A_{Sol,NC}$ for these two materials is very similar, most of the difference in their projected LSC performance can be attributed to the difference in η_{PL} . We note that the projected 2D flux gain for $\text{CuInS}_2/\text{CdS}$ NCs does not approach a maximum value even at unrealistically large sizes (80 m x 80 m, see SI), due to zero reabsorption of the lower energy part of the PL spectrum (Figure 1A). The performance of large-area LSCs containing these $\text{CuInS}_2/\text{CdS}$ NCs will therefore be limited by losses due to imperfections in the waveguides themselves that are not included in our model. Importantly, these $\text{CuInS}_2/\text{CdS}$ NCs are very small ($d = 3.1$ nm), so losses due to Rayleigh scattering by the NCs should be negligible.

The results presented here point to possible improvements in CuInS_2 -based NCs for LSC applications. Given the asymmetry of overlap between the $\text{CuInS}_2/\text{CdS}$ NC absorption and PL spectra, most of the photons that make it to the edge of a high-gain LSC containing $\text{CuInS}_2/\text{CdS}$ NCs will be from the lower energy half of the PL spectrum (Figure 2B). If this part of the PL spectrum lies beyond the peak of the solar-cell EQE spectrum, then the overall performance of the LSC device could be diminished. Preliminary simulations suggest, however, that marked improvements should be possible by narrowing the CuInS_2 NC band gap to ~ 670 nm because, down to this band gap, the gains in solar absorption are predicted to be greater than the performance losses due to reduction in overlap between the PL and Si EQE spectra. Unfortunately, experimental CuInS_2 -based NCs with narrower band gaps have so far shown only substantially smaller η_{PL} values (e.g., $\eta_{PL} < \sim 0.3$ for CuInS_2 NCs with $\lambda_{\text{thresh}} > \sim 600$ nm),^{20,25} but improvements in surface passivation or development of entirely new synthesis methods²⁶ may offer opportunities to reach this goal. Among CuInS_2 -based NCs reported to date, the $\text{CuInS}_2/\text{CdS}$ NCs shown in Figure 1 have close to the best balance of performance parameters attainable.

The results presented here also provide motivation for developing copper-doped nanocrystals with higher η_{PL} . $\text{Cd}_{1-x}\text{Cu}_x\text{Se}$ NCs like those described in ref. 16 (and summarized here) but with η_{PL} like the $\text{CuInS}_2/\text{CdS}$ NCs described here would show even greater flux gains than these $\text{CuInS}_2/\text{CdS}$ NCs because of their substantially smaller reabsorption losses. The synthesis of copper-doped nanocrystals with such high η_{PL} remains a challenge.

In summary, bright ($\eta_{PL} = 0.86$) $\text{CuInS}_2/\text{CdS}$ NCs have been demonstrated to be attractive phosphors for high-gain full-spectrum LSC applications. Their broad solar absorption and high PL quantum yields combine to outweigh their moderate reabsorption losses, and lead $\text{CuInS}_2/\text{CdS}$ NCs to outperform $\text{Cd}_{0.999}\text{Cu}_{0.001}\text{Se}$ NCs that have smaller reabsorption losses but much lower PL quantum yields. High-gain planar LSCs based on these $\text{CuInS}_2/\text{CdS}$ NCs are currently under development. More generally, these results further validate the use of both the 1D LSC device and the calculation of reabsorption probabilities using equation 1 for rapid assessment of critical performance characteristics of new LSC luminophores. By specifically

focusing on quantitative assessment of new luminophores, such approaches may help accelerate the development of next-generation luminophores for use in a broad variety of future LSC technologies.

Financial support from the U.S. National Science Foundation (DMR-1206221 to D.R.G. and DMR-1035512 to S. M.) and the U.S. Department Of Energy (Office of Energy Efficiency and Renewable Energy (DOE-EERE) Postdoctoral Research Award to K.E.K.) is gratefully acknowledged.

^a Department of Chemistry, University of Washington, Seattle, Washington 98195-1700, United States. E-mail: gamelin@chem.washington.edu

^b Mathematics Department, Western Washington University, 516 High Street, Bellingham, Washington 98225, United States

† Electronic Supplementary Information (ESI) available: Experimental details for the synthesis and characterization of $\text{CuInS}_2/\text{CdS}$ NCs, spectroscopic measurements, and additional calculated results. See DOI: 10.1039/c000000x/

- J. S. Batchelder, A. H. Zewail and T. Cole, *Appl. Opt.*, 1979, **18**, 3090.
- M. G. Debije and P. P. C. Verbunt, *Adv. Energy Mater.*, 2012, **2**, 12.
- K. R. McIntosh, N. Yamada and B. S. Richards, *Appl. Phys. B: Lasers Opt.*, 2007, **88**, 285.
- J. Yoon, L. Li, A. V. Semichayevsky, J. H. Ryu, H. T. Johnson, R. G. Nuzzo and J. A. Rogers, *Nature Commun.*, 2011, **2**, 343.
- Y. Shen, Y. Jia, X. Sheng, L. Shen, J. A. Rogers and N. C. Giebink, *ACS Photonics*, 2014, **1**, 746.
- R. Reisfeld, D. Shamrakov and C. Jorgensen, *Sol. Energy Mater. Sol. Cells*, 1994, **33**, 417.
- D. K. G. de Boer, D. J. Broer, M. G. Debije, W. Keur, A. Meijerink, C. R. Ronda and P. P. C. Verbunt, *Opt. Express*, 2012, **20**, A395.
- G. V. Shcherbatyuk, R. H. Inman, C. Wang, R. Winston and S. Ghosh, *Appl. Phys. Lett.*, 2010, **96**, 191901.
- J. Bomm, A. Buchtemann, A. J. Chatten, R. Bose, D. J. Farrell, N. L. A. Chan, Y. Xiao, L. H. Slooff, T. Meyer, A. Meyer, W. G. J. H. M. van Sark and R. Kooze, *Sol. Energy Mater. Sol. Cells*, 2011, **95**, 2087.
- R. H. Inman, G. V. Shcherbatyuk, D. Medvedko, A. Gopinathan and S. Ghosh, *Opt. Express*, 2011, **19**, 24308.
- F. Purcell-Milton and Y. K. Gun'ko, *J. Mater. Chem.*, 2012, **22**, 16687.
- Z. Krumer, S. J. Pera, R. J. A. van Dijk-Moes, Y. Zhao, A. F. P. de Brouwer, E. Groeneveld, W. G. J. H. M. van Sark, R. E. I. Schropp and C. de Mello Donega, *Sol. Energy Mater. Sol. Cells*, 2013, **111**, 57.
- F. Meinardi, A. Colombo, K. A. Velizhanin, R. Simonutti, M. Lorenzon, L. Beverina, R. Viswanatha, V. I. Klimov and S. Brovelli, *Nat. Photonics*, 2014, **8**, 392.
- I. Coropceanu and M. G. Bawendi, *Nano Lett.*, 2014, **14**, 4097.
- C. S. Erickson, L. R. Bradshaw, S. McDowall, J. D. Gilbertson, D. R. Gamelin and D. L. Patrick, *ACS Nano*, 2014, **8**, 3461.
- L. R. Bradshaw, K. E. Knowles, S. McDowall and D. R. Gamelin, *Nano Lett.*, 2015, **15**, 1315.
- M. J. Currie, J. K. Mapel, T. D. Heidel, S. Goffri and M. A. Baldo, *Science*, 2008, **321**, 226.
- M. Hammam, M. K. El-Mansy, S. M. El-Bashir and M. G. El-Shaarawy, *Desalination*, 2007, **209**, 244.
- N. D. Bronstein, L. F. Li, L. Xu, Y. Yao, V. E. Ferry, A. P. Alivisatos and R. G. Nuzzo, *ACS Nano*, 2014, **8**, 44.
- L. Li, A. Pandey, D. J. Werder, B. P. Khanal, J. M. Pietryga and V. I. Klimov, *J. Am. Chem. Soc.*, 2011, **133**, 1176.
- M. A. Green, K. Emery, Y. Hishikawa, W. Warta and E. D. Dunlop, *Prog. Photovoltaics*, 2014, **22**, 701.
- J. J. M. Binsma, L. J. Giling and J. Bloem, *J. Lumin.*, 1982, **27**, 35.
- H. Nakamura, W. Kato, M. Uehara, K. Nose, T. Omata, S. Otsuka-Yao-Matsuo, M. Miyazaki and H. Maeda, *Chem. Mater.*, 2006, **18**, 3330.
- Y.-K. Kim, S.-H. Ahn, K. Chung, Y.-S. Cho and C.-J. Choi, *J. Mater. Chem.*, 2012, **22**, 1516.
- R. Xie, M. Rutherford and X. Peng, *J. Am. Chem. Soc.*, 2009, **131**, 5691.
- W. van der Stam, A. C. Berends, F. T. Rabouw, T. Willhammar, X. Ke, J. D. Meeldijk, S. Bals and C. de Mello Donega, *Chem. Mater.*, 2015, **27**, 621.